

# Single-Layer Electroluminescent Devices and Photoinduced Hydrogen Production from an Ionic Iridium(III) Complex

Michael S. Lowry, Jonas I. Goldsmith,<sup>†</sup> Jason D. Slinker,<sup>‡</sup> Richard Rohl,<sup>‡</sup>  
Robert A. Pascal, Jr., George G. Malliaras,<sup>\*,‡</sup> and Stefan Bernhard\*

Department of Chemistry, Princeton University, Princeton, New Jersey 08544, Department of Chemistry, Bryn Mawr College, Bryn Mawr, Pennsylvania 19010, and Department of Materials Science and Engineering, Cornell University, Ithaca, New York 14853

Received June 17, 2005. Revised Manuscript Received August 30, 2005

We report the electronic structure and diverse applications of a highly luminescent ionic transition metal complex,  $[\text{Ir}(\text{dF}(\text{CF}_3)\text{ppy})_2(\text{dtbbpy})](\text{PF}_6)$  (where  $\text{dF}(\text{CF}_3)\text{ppy} = 2-(2,4\text{-difluorophenyl})-5\text{-trifluoromethylpyridine}$  and  $\text{dtbbpy} = 4,4'\text{-di-tert-butyl-2,2'-dipyridyl}$ ). The large HOMO–LUMO gap ( $\Delta E = 3.06$  V) enabled high-energy electroluminescence from the complex. Single-layer devices were fabricated and found to emit blue-green light (500 nm). The strong reducing strength of the excited state ( $E^*_{\text{ox}} = 1.21$  V) enabled effective catalysis of the photoinduced reduction of  $\text{H}_2\text{O}$  to  $\text{H}_2$ . It was found that the relative quantum yield of hydrogen was over an order of magnitude improved from the standard photosensitizer  $\text{Ru}(\text{dmpen})_3^{2+}$  ( $\text{dmpen} = 4,7\text{-dimethyl-1,10-phenanthroline}$ ).

## Introduction

Transition metal complexes are being explored for a multitude of optoelectronic and photocatalytic applications, including organic light emitting diodes (OLEDs),<sup>1–5</sup> photovoltaic cells,<sup>6–9</sup> and hydrogen production via the photoreduction of water.<sup>10–13</sup> The effectiveness of a transition metal complex in a specific role is determined by its photophysical and electrochemical properties, which depend on the electronic structure of its ligands and can be manipulated through deliberate chemical synthesis. In particular, ionic transition metal complexes (iTMCs) have emerged as promising

chromophoric materials due to their utility in single-layer electroluminescent devices.<sup>14–17</sup> The highly tunable, reversible redox properties of iTMCs and the ability to effectively harness radiant energy also distinguishes this class of materials as viable photosensitizers for catalyzing electron-transfer reactions.<sup>10,12,13,18–20</sup>

Single-layer electroluminescent devices are much more straightforward to fabricate than multilayer devices constructed of charge-neutral materials. In single-layer devices, electrons and holes are injected from two electrodes directly into the iTMC; emission takes place when the electrons and holes recombine. Unlike conventional, charge-neutral OLED materials, iTMCs contain mobile counterions that facilitate charge transport through the material and eliminate the need for electron- and hole-injection layers.<sup>15,21,22</sup> iTMC-based devices are also unique due to their ability to operate with air-stable electrodes, a phenomenon that can be attributed to the high electric fields that are produced by ions accumulating at the anode and cathode.<sup>15,16</sup> The emissive properties of these devices can be regulated through either internal or external parameters. For instance, device turn-on

\* To whom correspondence should be addressed. E-mail: george@cmr.cornell.edu (G.G.M.), sbernarh@princeton.edu (S.B.).

<sup>†</sup> Bryn Mawr College.

<sup>‡</sup> Cornell University.

- (1) Laskar, I. R.; Chen, T.-M. *Chem. Mater.* **2004**, *16*, 111.
- (2) Tsuboyama, A.; Iwawaki, H.; Furugori, M.; Mukaide, T.; Kamatani, J.; Igawa, S.; Moriyama, T.; Miura, S.; Takiguchi, T.; Okada, S.; Hoshino, M.; Ueno, K. *J. Am. Chem. Soc.* **2003**, *125*, 12971.
- (3) Adachi, C.; Baldo, M. A.; Thompson, M. E.; Forrest, S. R. *J. Appl. Phys.* **2001**, *90*, 5048.
- (4) Laskar, I. R.; Hsu, S.-F.; Chen, T.-M. *Polyhedron* **2005**, *24*, 189.
- (5) Lamansky, S.; Djurovich, P.; Murphy, D.; Abdel-Razzaq, F.; Kwong, R.; Tsyba, I.; Bortz, M.; Mui, B.; Bau, R.; Thompson, M. E. *Inorg. Chem.* **2001**, *40*, 1704.
- (6) Cook, M. J.; Lewis, A. P.; McAuliffe, G. S. G.; Skarda, V.; Thomson, A. J.; Glasper, J. L.; Robbins, D. J. *J. Chem. Soc., Perkin Trans. 2* **1984**, 1293.
- (7) Wong, H. L.; Lam, L. S. M.; Cheng, K. W.; Man, K. Y. K.; Chan, W. K.; Kwong, C. Y.; Djurišić, A. B. *Appl. Phys. Lett.* **2004**, *84*, 2557.
- (8) Hara, K.; Nishikawa, T.; Kurashige, M.; Kawachi, H.; Kashima, T.; Sayama, K.; Aika, K.; Arakawa, H. *Solar Energy Mater. Solar Cells* **2005**, *85*, 21.
- (9) Polo, A. S.; Itokazu, M. K.; Murakami Iha, N. Y. *Coord. Chem. Rev.* **2004**, *248*, 1343.
- (10) Goldsmith, J. I.; Hudson, W. R.; Lowry, M. S.; Anderson, T. H.; Bernhard, S. *J. Am. Chem. Soc.* **2005**, *127*, 7502.
- (11) Kalyanasundaram, K.; Kiwi, J.; Grätzel, M. *Helv. Chim. Acta* **1978**, *61*, 2720.
- (12) Kirch, M.; Lehn, J. M.; Sauvage, J. P. *Helv. Chim. Acta* **1979**, *62*, 1345.
- (13) Krishnan, C. V.; Brunschwig, B. S.; Creutz, C.; Sutin, N. *J. Am. Chem. Soc.* **1985**, *107*, 2005.

- (14) Barron, J. A.; Bernhard, S.; Houston, P. L.; Abruña, H. D.; Ruglovsky, J. L.; Malliaras, G. G. *J. Phys. Chem. A* **2003**, *107*, 8130.
- (15) Slinker, J.; Bernards, D.; Houston, P. L.; Abruña, H. D.; Bernhard, S.; Malliaras, G. G. *Chem. Commun.* **2003**, 2392.
- (16) Slinker, J. D.; Gorodetsky, A. A.; Lowry, M. S.; Wang, J.; Parker, S.; Rohl, R.; Bernhard, S.; Malliaras, G. G. *J. Am. Chem. Soc.* **2004**, *126*, 2763.
- (17) Lee, J.-K.; Yoo, D. S.; Handy, E. S.; Rubner, M. F. *Appl. Phys. Lett.* **1996**, *69*, 1686.
- (18) Schwarz, H. A.; Creutz, C.; Sutin, N. *Inorg. Chem.* **1985**, *24*, 433.
- (19) Lin, C.-T.; Böttcher, W.; Chou, M.; Creutz, C.; Sutin, N. *J. Am. Chem. Soc.* **1976**, *98*, 6536.
- (20) Kalyanasundaram, K. *Photochemistry of Polypyridine and Porphyrin Complexes*; Academic Press: San Diego, CA, 1992.
- (21) Buda, M.; Kalyuzhny, G.; Bard, A. J. *J. Am. Chem. Soc.* **2002**, *124*, 6090.
- (22) Gorodetsky, A. A.; Parker, S.; Slinker, J. D.; Bernards, D. A.; Wong, M. H.; Malliaras, G. G.; Flores-Torres, S.; Abruña, H. D. *Appl. Phys. Lett.* **2004**, *84*, 807.

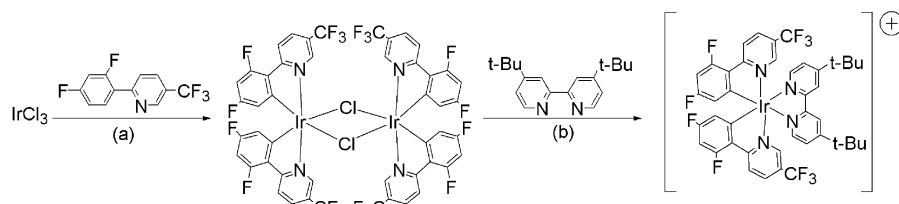


**Figure 1.** Synthesis of complex **1**. The final product is isolated as a  $\text{PF}_6^-$  salt and recrystallized by acetone:pentane vapor diffusion: (a)  $\text{CH}_3\text{OCH}_2\text{CH}_3:\text{H}_2\text{O}$  (2:1),  $120^\circ\text{C}$ , 12 h and (b)  $\text{HOCH}_2\text{CH}_2\text{OH}$ ,  $150^\circ\text{C}$ , 15 h.

time (the time it takes to reach maximum emission upon the application of a dc bias) can be adjusted either by modifying the ionic conductivity of the single-layer material<sup>23–26</sup> or by applying a gradient bias.<sup>24</sup>

The earliest reported single-layer transition metal-based devices were prepared with chelated ruthenium(II) complexes (e.g.,  $\text{Ru}(\text{bpy})_3^{2+}$ ), but these complexes emitted exclusively in the orange-red portion of the visible spectrum.<sup>14,26,27</sup> Since that time, the emission color of ionic ruthenium(II) complexes has not been tuned to higher energies.<sup>15</sup> Due to the fact that the emissive transition in such a complex takes place between a filled metal d-orbital and a vacant ligand  $\pi^*$  orbital,<sup>20</sup> the potential for color-tuning ruthenium(II) (and other second row transition metal) complexes to higher emission energies is limited by weak ligand-field splitting. By employing a more stable third-row transition element, such as rhenium(I),<sup>28,29</sup> osmium(II),<sup>30</sup> or iridium(III),<sup>1,31,32</sup> higher emission energies are attainable, likely owing to increased ligand-field stabilization energy (LFSE). In particular, iridium(III) is appealing because of its synthetic versatility<sup>2,5,31–33</sup> (it is able to form both homo- and heteroleptic complexes) as well as its tunable color in solution-based photoluminescence studies.<sup>34,35</sup>

Recently, efficient yellow<sup>16</sup> and green<sup>36</sup> electroluminescence were reported from single-layer devices that were fabricated using ionic iridium(III) complexes with the base structure  $[\text{Ir}(\text{ppy})_2(\text{bpy})]^+$  (where ppy = 2-phenylpyridine; bpy = 2,2'-dipyridyl). The precedent of color tuning neutral cyclometalated iridium(III) complexes suggests that judicious

ligand selection may lead to superior control over the emission properties of ionic iridium(III)-based devices.<sup>1,4,5,32,37</sup> The use of fluorinated cyclometalating ligands has been associated with a large HOMO–LUMO gap and high emission energy in electrochemical and luminescence studies involving both neutral and ionic iridium(III) complexes.<sup>5,38–41</sup> Similarly, the inclusion of an alkyl-substituted diimine group helps alleviate problems with charge-transport and self-quenching in solid state materials and is believed to contribute strongly to the occurrence of electroluminescence from single-layer iTMC-based devices.<sup>16,36,42,43</sup>

In addition to their ability to electroluminesce, iTMCs have also been examined for their ability to drive electron-transfer reactions.<sup>10–13,20</sup> Ruthenium(II) polypyridine photosensitizers have been shown to facilitate the photon-driven reduction of  $\text{H}_2\text{O}$  to  $\text{H}_2$  because of the strong reducing ability of their excited states.<sup>10–13,19,20</sup> We have recently used ligand modification techniques to develop heteroleptic, ionic iridium(III) complexes with enhanced photocatalytic properties.<sup>10</sup> The complementarity between suitable OLED materials and those that would effectively catalyze the photoreduction of water is clear, inasmuch as efficient energy conversion and long excited state lifetimes are mutually desirable.

Following previously reported ligand-based trends,<sup>10,16,32,34,36,40</sup> we have chosen to tailor the photophysical and electroluminescent properties of an ionic material by synthetic design. We report herein the synthesis, characterization, electronic structure, and photocatalytic and optoelectronic applications of  $[\text{Ir}(\text{dF}(\text{CF}_3)\text{ppy})_2(\text{dtbbpy})](\text{PF}_6)$ , complex **1** (where  $\text{dF}(\text{CF}_3)\text{ppy}$  = 2-(2,4-difluorophenyl)-5-trifluoromethylpyridine and dtbbpy = 4,4'-di-*tert*-butyl-2,2'-dipyridyl) (Figure 1). The heavily fluorinated cyclometalating ligand and sterically bulky neutral ligand were selected to optimize the photophysical properties of the material and to increase its efficacy in multifarious applications.

## Experimental Section

**General.**  $^1\text{H}$  and  $^{13}\text{C}$  NMR spectra were recorded on a Varian Inova-500 spectrometer at room temperature. Mass spectral data

- (23) Parker, S. T.; Slinker, J. D.; Lowry, M. S.; Cox, M. P.; Bernhard, S.; Malliaras, G. G. *Chem. Mater.* **2005**, *17*, 3187.  
 (24) Lyons, C. H.; Abbas, E. D.; Lee, J.-K.; Rubner, M. F. *J. Am. Chem. Soc.* **1998**, *120*, 12100.  
 (25) Leprêtre, J.-C.; Deronzier, A.; Stéphan, O. *Synth. Met.* **2002**, *131*, 175.  
 (26) Gao, F. G.; Bard, A. J. *J. Am. Chem. Soc.* **2000**, *122*, 7426.  
 (27) Handy, E. S.; Pal, A. J.; Rubner, M. F. *J. Am. Chem. Soc.* **1999**, *121*, 3525.  
 (28) Li, F.; Zhang, M.; Cheng, G.; Feng, J.; Zhao, Y.; Ma, Y.; Liu, S.; Shen, J. *Appl. Phys. Lett.* **2004**, *84*, 148.  
 (29) Ranjan, S.; Lin, S.-Y.; Hwang, K.-C.; Chi, Y.; Ching, W.-L.; Liu, C.-S.; Tao, Y.-T.; Chien, C.-H.; Peng, S.-M.; Lee, G.-H. *Inorg. Chem.* **2003**, *42*, 1248.  
 (30) Bernhard, S.; Gao, X.; Malliaras, G. G.; Abruña, H. D. *Adv. Mater.* **2002**, *14*, 433.  
 (31) Neve, F.; La Deda, M.; Crispini, A.; Bellusci, A.; Puntoriero, F.; Campagna, S. *Organometallics* **2004**, *23*, 5856.  
 (32) Lamansky, S.; Djurovich, P.; Murphy, D.; Abdel-Razzaq, F.; Lee, H.-E.; Adachi, C.; Burrows, P. E.; Forrest, S. R.; Thompson, M. E. *J. Am. Chem. Soc.* **2001**, *123*, 4304.  
 (33) Neve, F.; Crispini, A.; Campagna, S.; Serroni, S. *Inorg. Chem.* **1999**, *38*, 2250.  
 (34) Lowry, M. S.; Hudson, W. R.; Pascal, R. A., Jr.; Bernhard, S. *J. Am. Chem. Soc.* **2004**, *126*, 14129.  
 (35) Coppo, P.; Duati, M.; Kozhevnikov, V. N.; Hofstraat, J. W.; De Cola, L. *Angew. Chem., Int. Ed.* **2005**, *44*, 1806.  
 (36) Slinker, J. D.; Koh, C. Y.; Malliaras, G. G.; Lowry, M. S.; Bernhard, S. *Appl. Phys. Lett.* **2005**, *86*, 173506.

- (37) Pohl, R.; Montes, V. A.; Shinar, J.; Anzenbacher, P., Jr. *J. Org. Chem.* **2004**, *69*, 1723.  
 (38) Wang, Y.; Herron, N.; Grushin, V. V.; LeCloux, D.; Petrov, V. *Appl. Phys. Lett.* **2001**, *79*, 449.  
 (39) Tamayo, A. B.; Alleyne, B. D.; Djurovich, P. I.; Lamansky, S.; Tsyba, I.; Ho, N. N.; Bau, R.; Thompson, M. E. *J. Am. Chem. Soc.* **2003**, *125*, 7377.  
 (40) Coppo, P.; Plummer, E. A.; De Cola, L. *Chem. Commun.* **2004**, 1774.  
 (41) Chang, W.-C.; Hu, A. T.; Duan, J.-P.; Rayabarapu, D. K.; Cheng, C.-H. *J. Organomet. Chem.* **2004**, *689*, 4882.  
 (42) Bernhard, S.; Barron, J. A.; Houston, P. L.; Abruña, H. D.; Ruglovsky, J. L.; Gao, X.; Malliaras, G. G. *J. Am. Chem. Soc.* **2002**, *124*, 13624.  
 (43) Rudmann, H.; Shimada, S.; Rubner, M. F. *J. Am. Chem. Soc.* **2002**, *124*, 4918.

were collected using a Hewlett-Packard 5898B (Electrospray) MS engine.

All photophysical characterizations were conducted at room temperature using a 25  $\mu$ M acetonitrile solution of complex **1**, which was purged with N<sub>2</sub> in a capped quartz cuvette (1.0 cm) for 10 min prior to analysis. UV-visible electronic absorption spectra were recorded using a Hewlett-Packard 8453 diode-array spectrometer. Photoluminescence spectra were recorded on a Jobin-Yvon Fluorolog-3 spectrometer equipped with dual monochromators and a Hamamatsu-928 photomultiplier tube (PMT) at right angle geometry. Each emission spectrum was recorded at an excitation wavelength of 400 nm and was corrected according to the calibration factors of the instrument. The photoluminescent quantum yield ( $\Phi_{\text{PL}}$ ) of complex **1** was determined relative to that of Ru(bpy)<sub>3</sub><sup>2+</sup> in acetonitrile [25  $\mu$ M] at room temperature ( $\Phi_{\text{PL}}$  = 6.2%). Excited-state lifetimes ( $\tau$ ) were measured using the emission monochromator and PMT detector of the Jobin-Yvon Fluorolog-3 spectrometer. Complex **1** was excited at 337 nm with an N<sub>2</sub> laser (Laser Science, Inc. VSL-337LRF, 10 ns pulse), and the emission decay was recorded using a Tektronix TDS 3032B digital phosphor oscilloscope. Thin film samples (200 nm) were prepared by spin-coating (2500 rpm) complex **1** from an acetonitrile solution (30 mg/mL) onto a quartz disk. Corrected emission spectra were recorded using the Jobin-Yvon Fluorolog-3 spectrometer with front-face detection at an excitation wavelength of 400 nm.

Redox potentials of complex **1**, along with those of three reference ionic iridium(III) complexes {[Ir(C $\wedge$ N)<sub>2</sub>(dtbbpy)]<sup>+</sup>, where C $\wedge$ N = ppy, 2-(4-fluorophenyl)-5-methylpyridine (Fmppy), or 2-(2,4-difluorophenyl)-5-methylpyridine (dFmppy)}, were determined by cyclic voltammetry (CV) using an EG&G PAR 273A potentiostat/galvanostat at a potential sweep rate of 100 mV/s. A homemade platinum disk electrode served as the working electrode, a coiled platinum wire was used as the counter electrode, and a silver wire was used as a quasi-reference electrode. Electrochemical measurements were carried out in a home-built one-compartment cell at approximately 1 mM concentration of iridium(III) complex in 0.1 M tetra-*n*-butylammonium hexafluorophosphate (TBAH) in acetonitrile. Solutions were purged with nitrogen for 10 min prior to each measurement to ensure that they were oxygen-free. Ferrocene was added as an internal standard ( $E^{\circ}$  = 0.31 V),<sup>44</sup> and all potentials were subsequently referenced to SCE.

**Materials.** 2,4-Difluorophenylboronic acid, tetrakis(triphenylphosphine)palladium(0) (PdL<sub>4</sub>), ferrocene, triethanolamine (TEOA), 4,4'-di-*tert*-butyl-2,2'-dipyridyl (dtbbpy), and iridium(III) chloride hydrate were obtained from Aldrich and used as received. 2-Chloro-5-(trifluoromethyl)pyridine was obtained from Acros Organics and also used as received. Tetra-*n*-butylammonium hexafluorophosphate (TBAH, electrochemical grade) and electrochemical grade acetonitrile (>99.5% over molecular sieves) were obtained from Fluka and used as received. Several compounds, such as Ru(bpy)<sub>3</sub><sup>2+</sup>,<sup>42</sup> Ru(dmphen)<sub>3</sub><sup>2+</sup><sup>19</sup> (where dmphen = 4,7-dimethyl-1,10-phenanthroline), and [Co(bpy)<sub>3</sub>]Cl<sub>2</sub><sup>10</sup> were synthesized according to previously reported literature procedures. [Ir(ppy)<sub>2</sub>(dtbbpy)]<sup>+</sup><sup>16</sup> and [Ir(Fmppy)<sub>2</sub>(dtbbpy)]<sup>+</sup><sup>36</sup> have also been reported and were prepared by cleavage of a cyclometalated dichloro-bridged diiridium dimer with dtbbpy in ethylene glycol at 150 °C. [Ir(dFmppy)<sub>2</sub>(dtbbpy)]<sup>+</sup> was prepared in an analogous manner to [Ir(ppy)<sub>2</sub>(dtbbpy)]<sup>+</sup> and [Ir(Fmppy)<sub>2</sub>(dtbbpy)]<sup>+</sup>.

**Synthesis of dF(CF<sub>3</sub>)ppy.** A mixture of 2-chloro-5-(trifluoromethyl)pyridine (3.0 mmol, 0.68 g), 2,4-difluorophenylboronic acid (3.3 mmol, 0.52 g), and PdL<sub>4</sub> (0.070 mmol, 0.081 g) in benzene (4.0 mL), 2.0 M aqueous sodium carbonate (3.0 mL), and ethanol

(0.75 mL) was stirred and heated to reflux (70 °C) under nitrogen for 48 h. After cooling to room temperature, the reaction mixture was transferred to a separatory funnel with water (3  $\times$  25 mL) and dichloromethane (15 mL) and the organic layer was separated. The aqueous layer was extracted with dichloromethane (2  $\times$  20 mL). The combined organic layers were washed with water (50 mL) and filtered through silica gel over a porous glass frit using additional dichloromethane as eluent. The collected filtrate was dried over Na<sub>2</sub>SO<sub>4</sub>(s) and concentrated to dryness under reduced pressure at 65 °C, yielding a pale yellow-green solid, dF(CF<sub>3</sub>)ppy. Yield: 0.70 g (90%). <sup>1</sup>H NMR (500 MHz, CDCl<sub>3</sub>): 8.99 (s, 1 H, pyridyl-H<sup>6</sup>), 8.09–8.14 (m, 1 H, phenyl-H<sup>5</sup>), 8.01 (d, 1 H,  $J$  = 9 Hz, pyridyl-H<sup>4</sup>), 7.93 (d, 1 H,  $J$  = 8 Hz, pyridyl-H<sup>3</sup>), 7.06 (td, 1 H,  $J$  = 8 Hz, 1 Hz, phenyl-H<sup>6</sup>), 6.97 (t, 1 H,  $J$  = 9 Hz, phenyl-H<sup>3</sup>). <sup>13</sup>C NMR (125 MHz, CDCl<sub>3</sub>): 165.2, 163.2, 162.2, 160.2, 155.9, 146.8, 134.1, 132.7, 125.6, 123.9, 112.6, 105.1. MS ( $m/e$ , ESI): 260 (100, M<sup>+</sup> + H).

**Synthesis of [(dF(CF<sub>3</sub>)ppy)<sub>2</sub>-Ir- $\mu$ -Cl]<sub>2</sub>.** Iridium(III) chloride hydrate (0.30 mmol, 0.089 g) was added to a solution of 2-(2,4-difluorophenyl)-5-trifluoromethylpyridine (0.68 mmol, 0.18 g) in 2-methoxyethanol (4.0 mL) and water (2.0 mL). The reaction mixture was heated to reflux (120 °C) under nitrogen with constant stirring for 12 h. Upon cooling to room temperature, an amorphous green precipitate formed. The resulting green powder was collected via filtration, washed with water (3  $\times$  20 mL), dried, and recrystallized from a methanol:acetone solution (4:1) to yield the pure product, [(dF(CF<sub>3</sub>)ppy)<sub>2</sub>-Ir- $\mu$ -Cl]<sub>2</sub>. Yield: 0.20 g (89%). <sup>1</sup>H NMR (500 MHz, CDCl<sub>3</sub>): 9.50 (d, 4 H,  $J$  = 1 Hz, pyridyl-H<sup>6</sup>), 8.45 (dd, 4 H,  $J$  = 9 Hz, 3 Hz, pyridyl-H<sup>4</sup>), 8.04 (dd, 4 H,  $J$  = 9 Hz, 2 Hz, pyridyl-H<sup>3</sup>), 6.39–6.47 (m, 4 H, phenyl-H<sup>5</sup>), 5.06 (dd, 4 H,  $J$  = 9 Hz, 2 Hz, phenyl-H<sup>2</sup>).

**Synthesis of [Ir(dF(CF<sub>3</sub>)ppy)<sub>2</sub>(dtbbpy)](PF<sub>6</sub>) (**1**).** Bis-( $\mu$ -chlorotetrakis(2-(4,6-difluoromethylphenyl)-pyridinato-C<sub>2</sub>,N)diiridium(III) (0.09 mmol, 0.13 g) was heated to reflux (150 °C) with 4,4'-di-*tert*-butyl-2,2'-dipyridyl (0.20 mmol, 0.054 g) in ethylene glycol (6.0 mL) under nitrogen with constant stirring for 15 h. Upon cooling to room temperature, the mixture was transferred to a separatory funnel with water (60 mL) and washed with hexanes (3  $\times$  30 mL). The aqueous layer was heated to 85 °C for 5 min to remove residual hexanes. A 10 mL aqueous ammonium hexafluorophosphate solution (1.0 g in 10 mL deionized water) was added to the reaction mixture, producing a yellow-green amorphous powder. This precipitate was filtered, dried, and recrystallized by acetone:pentane vapor diffusion, giving the pure product **1**, [Ir(dF(CF<sub>3</sub>)ppy)<sub>2</sub>(dtbbpy)](PF<sub>6</sub>). Yield: 0.15 g (75%). <sup>1</sup>H NMR (500 MHz, acetone-*d*<sub>6</sub>): 8.97 (d, 2 H,  $J$  = 2 Hz, dF(CF<sub>3</sub>)ppy, pyridyl-H<sup>6</sup>), 8.64 (dd, 2 H,  $J$  = 9 Hz, 3 Hz, dtbbpy-H<sup>6</sup>), 8.43 (dd, 2 H,  $J$  = 9 Hz, 2 Hz, dtbbpy-H<sup>5</sup>), 8.20 (d, 2 H,  $J$  = 6 Hz, dF(CF<sub>3</sub>)ppy, pyridyl-H<sup>4</sup>), 7.83–7.85 (m, 4 H, dtbbpy-H<sup>3</sup> and dF(CF<sub>3</sub>)ppy, pyridyl-H<sup>3</sup>), 6.89 (td, 2 H,  $J$  = 9 Hz, 2 Hz, dF(CF<sub>3</sub>)ppy, phenyl-H<sup>5</sup>), 6.00 (dd, 2 H,  $J$  = 9 Hz, 2 Hz, dF(CF<sub>3</sub>)ppy, phenyl-H<sup>3</sup>), 1.47 (s, 18 H). <sup>13</sup>C (125 MHz, acetone-*d*<sub>6</sub>): 168.2, 165.7, 156.3, 156.0, 151.4, 146.0, 137.5, 127.1, 126.3, 125.7, 125.4, 124.3, 124.1, 122.9, 114.8, 114.7, 99.7, 36.0, 17.7. MS ( $m/e$ , ESI): 978 (100, M<sup>+</sup> - PF<sub>6</sub><sup>-</sup> + H).

**Static DFT Calculations.** Hybrid density functional calculations (B3LYP/LANL2DZ) were performed by using GAUSSIAN 98.<sup>45</sup> The built-in default thresholds for gradient convergence were employed, but the threshold for wave function convergence was slightly relaxed [SCF=(CONVER=7)]. All geometry optimizations were carried out under the constraint of C<sub>2</sub> symmetry.

**Fabrication and Characterization of Light-Emitting Device.** Amorphous thin films of complex **1** were formed by spin-casting

(44) Bard, A. J.; Faulkner, L. R. *Electrochemical Methods: Fundamentals and Applications*; John Wiley & Sons: New York, 2001; p 811.

(45) Frisch, M. J.; et al. *Gaussian 98*; Gaussian, Inc.: Pittsburgh, 1998.

from acetonitrile solution (24 mg/mL) onto glass substrates with prepatterned ITO contacts (Thin Film Devices, Anaheim, CA) at 1000 rpm inside of a nitrogen glovebox. The thickness of the film (ca. 70–80 nm) was determined with profilometry. The ITO substrates were cleaned just before the deposition of the organic layer by a deionized water bath, followed by UV/ozone treatment. The films were taken out of the glovebox and dried for 12 h at 80 °C under vacuum. They were then reintroduced to the glovebox for further processing and characterization. The top contacts consisted of a 200 Å thick Au film, or a 10 Å CsF film capped with a 200 Å Al film. They were deposited with a shadow-mask that defined six devices per substrate, each with a 3 mm<sup>2</sup> active area. The deposition of Au was carried out intermittently to minimize heating of the organic film. The electrical characteristics of the devices were measured with a Keithley 236 source-measure unit, and the emission was collected with a calibrated UDT S370 optometer coupled to an integrating sphere. The electroluminescent spectra were measured with a calibrated S2000 Ocean Optics fiber spectrometer.

**Photogeneration of Hydrogen.** Complex **1** and Ru(dmphen)<sub>3</sub><sup>2+</sup> were used as photosensitizers for photoinduced hydrogen production in a reaction system that has been reported elsewhere.<sup>10</sup> Samples were prepared in 20-mL screw-cap glass vials (VWR) with silicone/PTFE septa. Each sample was made up to a volume of 10 mL in (1:1) aqueous acetonitrile. Samples typically contained 1.5 μmol of the photosensitizer, 50 μmol of Co(bpy)<sub>3</sub>Cl<sub>2</sub> (the electron relay), 2.7 mmol (115 mg) of LiCl, and 5.7 mmol (0.75 mL) of TEOA (the sacrificial reductant). 125 μL of 37% HCl was added to each solution to adjust the pH downward. Sample vials were capped and deoxygenated by bubbling nitrogen through them for 15 min. The samples were degassed under vacuum, through the septum on the vial, at ambient temperature for 30 min to remove all of the dissolved nitrogen. All hydrogen production was carried out with the vials still under vacuum. The vials were then placed in a home-built 16-compartment sample holder and illuminated from below using ultrabright light emitting diodes (Luxeon V Dental Blue, Future Electronics).

These LEDs have a luminous output of 500 mW ± 10% at 465 nm with a 20 nm fwhm and are driven at 700 mA using a Xitanium driver (Advance Transformer Co.). Each LED is mounted on a copper plate and the entire 16-well apparatus sits atop a water-cooled aluminum block. The whole apparatus (vials, holder, LEDs) is situated on an orbital shaker, shaken at 150 rpm, and illuminated for 40 h. After illumination, the sample vials were backfilled with water to bring them to ambient pressure, and 1.0 mL of the bubble of gas trapped in the vial was sampled using a Hamilton Sample-Lock syringe. This gas sample was injected into a home-built sample chamber in which a hydrogen sensor (H2Scan, RobustHydrogenSensor) was mounted. The sensor was connected to a PC, and data were collected using an interface designed in Labview. Prior to each sample injection, the sample chamber was purged with dry nitrogen until the output of the hydrogen sensor returned to its baseline reading (ca. 2 min). Typically, readings were taken 65 s after sample injection to allow the system to equilibrate. Daily calibrations were performed to ensure the accuracy of the sensor.

## Results and Discussion

**Synthesis.** dF(CF<sub>3</sub>)ppy was prepared by coupling 2-chloro-5-(trifluoromethyl)pyridine with 2,4-difluorophenylboronic acid in the presence of a palladium catalyst (PdL<sub>4</sub>) following a modified Suzuki pathway.<sup>46–49</sup> Excess arylboronic acid was

**Table 1. Photophysical Properties of Complex 1<sup>a</sup>**

absorption	$\lambda_{\text{abs}}$ (log $\epsilon$ )/nm	260 (4.74), 310 (4.53), 380 (3.79)
emission	$\lambda_{\text{em}}$ /nm	470
	$\tau$ /μs	2.3
	$\Phi_{\text{PL}}/\%$	68 <sup>b</sup>

<sup>a</sup> 25 μM acetonitrile solution. <sup>b</sup> Ru(bpy)<sub>3</sub><sup>2+</sup> was used as a reference ( $\Phi_{\text{PL}}$  6.2%).

removed from the reaction mixture by aqueous extraction. Residual catalyst was separated by filtering the sample through silica gel with dichloromethane. No further purification was required.

Complex **1** was prepared by coordinating two cyclometalating (C $\wedge$ N, dF(CF<sub>3</sub>)ppy) and one neutral (N $\wedge$ N, dtbbpy) ligand to an iridium(III) metal center according to the reaction pathway shown in Figure 1. In short, a cyclometalated dichloro-bridged diiridium dimer was formed and subsequently cleaved with a neutral, chelating dtbbpy ligand. The final product was isolated as a PF<sub>6</sub><sup>-</sup> salt and recrystallized, yielding a yellow-green powder.

**Photophysical Properties.** In iridium(III) complexes with the ppy–bpy scaffold, emission is derived from a mixed excited-state involving <sup>3</sup>MLCT ( $t_{2g} \rightarrow \pi^*_{\text{N}\wedge\text{N}}$ ) and <sup>3</sup>LC ( $\pi_{\text{C}\wedge\text{N}} \rightarrow \pi^*_{\text{C}\wedge\text{N}}$ ) transitions.<sup>50–52</sup> The emitted light can be described by the wave equation ( $\phi$ )<sup>2</sup>

$$\phi = a\phi(^3\text{MLCT}) + b\phi(^3\text{LC}) \quad (1)$$

where  $a$  and  $b$  are normalized coefficients that account for the contribution of <sup>3</sup>MLCT and <sup>3</sup>LC transitions to the observed emission.<sup>2</sup> As  $a < b$ , the emitted light has greater ligand-centered character, which is reflected in the shape (vibrationally structured) and position (hypsochromic shift) of the emission band.<sup>2,34</sup>

Photophysical data for complex **1** in solution are collected in Table 1. The UV–visible absorption profile and emission spectra for the complex in acetonitrile solution (25 μM) and as a thin film (200 nm) are shown in Figure 2. There are three prominent bands in the absorption spectrum of complex **1**: two intense bands in the ultraviolet region of the spectrum ( $\lambda_{\text{abs}} = 257, 298$  nm) and one broad, weak band centered at 378 nm, corresponding to two <sup>1</sup>LC transitions and one <sup>1</sup>MLCT transition, respectively (as identified by band location, size, and molar extinction coefficient).<sup>1,40</sup> Intersystem crossing from the singlet to the triplet state is enabled by strong spin–orbit coupling.<sup>20,53,54</sup>

Complex **1** emits in the blue-green (470 nm) portion of the visible spectrum with a quantum yield of 68% in solution. The thin-film emission spectrum for complex **1** is bathochromically shifted (501 nm) from the solution-based

- (47) Ali, N. M.; McKillop, A.; Mitchell, M. B.; Rebelo, R. A.; Wallbank, P. J. *Tetrahedron* **1992**, *48*, 8117.  
 (48) Grushin, V.; Lecloux, D. D.; Petrov, V. A.; Wang, Y. U.S. Patent Appl. Publ. US 2002190250, 2002.  
 (49) Petrov, V. A.; Wang, Y.; Grushin, V. PCT Int. Appl. WO 2002002714, 2002.  
 (50) Colombo, M. G.; Hauser, A.; Güdel, H. U. *Inorg. Chem.* **1993**, *32*, 3088.  
 (51) Colombo, M. G.; Güdel, H. U. *Inorg. Chem.* **1993**, *32*, 3081.  
 (52) Wilde, A. P.; King, K. A.; Watts, R. J. *J. Phys. Chem.* **1991**, *95*, 629.  
 (53) Turro, N. J. *Modern Molecular Photochemistry*; Benjamin/Cummings Pub. Co.: Menlo Park, CA, 1978.  
 (54) Valeur, B. *Molecular Fluorescence: Principles and Applications*; Wiley-VCH: Weinheim, Germany, 2002.

(46) Watanabe, T.; Miyaura, N.; Suzuki, A. *Synlett* **1992**, 207.

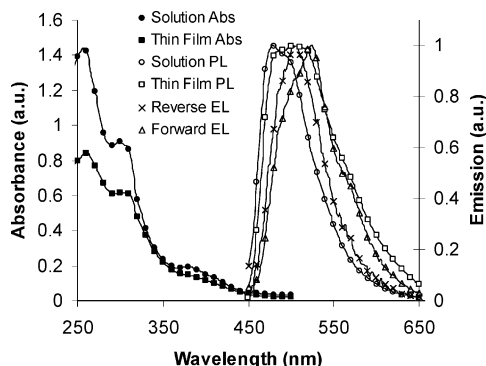


**Figure 2.** Absorption and emission spectra for complex **1**. Absorption spectra are presented for complex **1** in solution (●) and as a solid film (■). Emission spectra are presented for solution-based photoluminescence (○), thin film photoluminescence (□), and solid-state electrochromic luminescence (EL) under forward (△) and reverse (×) bias.

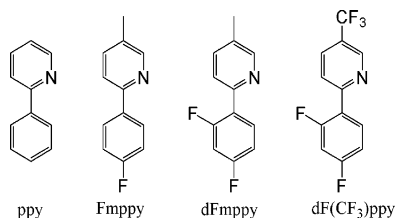


**Figure 3.** Structural evolution of  $dF(CF_3)ppy$  from ppy.

spectrum. This behavior is expected due to the increased degree of  $\pi$ -conjugation and orbital overlap for materials in the solid-state. By comparison,  $[Ir(ppy)_2(dtbbpy)](PF_6)$  and  $[Ir(Fmppy)_2(dtbbpy)](PF_6)$ —two previously reported electrochromic luminophores—emit at 567 and 543 nm in acetonitrile solution, respectively, with considerably lower photoluminescent quantum yields (14% and 26%).<sup>16,34,36</sup> Additionally, the excited-state lifetime of complex **1** (2.3  $\mu$ s) is much longer than that of the other iridium(III)—dtbbpy complexes (0.60  $\mu$ s for  $[Ir(ppy)_2(dtbbpy)](PF_6)$  and 1.1  $\mu$ s for  $[Ir(Fmppy)_2(dtbbpy)](PF_6)$ ).<sup>16,34,36</sup> These photoluminescent properties demonstrate the efficacy of complex **1** at collecting, storing, and emitting light energy and thus suggest that it has the potential to function well as both an electrochromic and an iTMC photosensitizer.

**Electrochemical Properties.** To ascertain the effects of individual substituent changes on the redox behavior of an iridium(III) dtbbpy-containing complex, cyclic voltammetry experiments were performed on four dtbbpy complexes whose structures represent the evolution of  $dF(CF_3)ppy$  from ppy (Figure 3). All four complexes within this series exhibited reversible redox behavior at a scan-rate of 100 mV/s; the CV of complex **1** can be seen in Figure 4. The redox wave (A) corresponds to the metal centered  $Ir^{III/IV}$  process; this oxidation is analogous to removing an electron from the metal centered HOMO. The redox wave (B) corresponds to the ligand-based  $dtbbpy^{0/-}$  process and is equivalent to the addition of an electron to the dtbbpy-centered LUMO. The energy gap between these two redox waves, therefore, approximates a <sup>1</sup>MLCT transition and can be directly related to the emission energy of the complex, as shown in Figure 5. The energy gap measured through electrochemistry is observed to be consistently larger than the emission energy due to Franck–Condon contributions from intra- and intermolecular reorganization, including changes in solvation.<sup>20</sup>

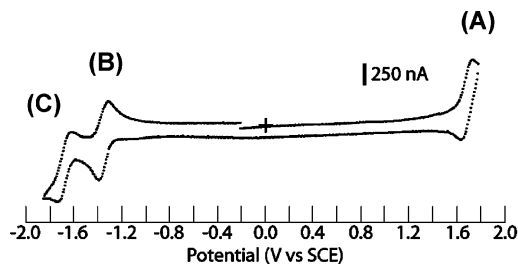


**Figure 4.** Cyclic voltammogram of complex **1** in 0.1 M TBAH/ $CH_3CN$  at a Pt working electrode with a Pt counter electrode and Ag wire quasi-reference. Ferrocene was used as an internal standard; potential sweep rate was 100 mV/s. (A)  $Ir^{III/IV}$  (B)  $dtbbpy^{0/-}$  (C)  $dF(CF_3)ppy^{-/-2}$

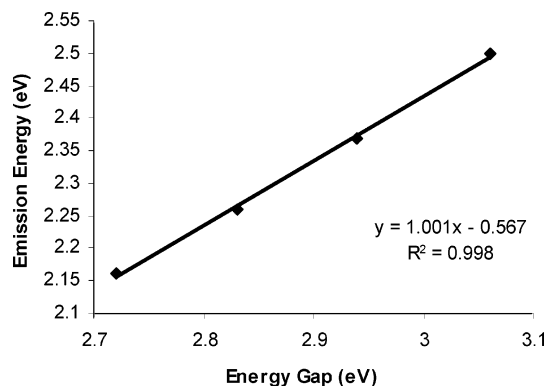


**Figure 5.** A linear relationship exists between the emission energy (from solution-based photoluminescence studies) and the experimentally determined energy gap (calculated from redox potentials) for the  $[Ir(C\wedge N)_2(dtbbpy)](PF_6)$  series  $\{C\wedge N = ppy, Fmppy, dFmppy, dF(CF_3)ppy\}$ . The nonzero intercept can be attributed to Franck–Condon contributions.

As exemplified by the redox potentials listed in Table 2, adding fluoro substituents to the cyclometalating ligand has a dramatic effect on the LFSE of iridium(III) complexes. The strongly electron-withdrawing fluoro substituents pull electron density away from the metal center, thereby stabilizing the metal d-orbitals and making it more difficult to oxidize the metal center. Consequently, the potential of the metal-centered redox process increases by nearly 500 mV upon transitioning from ppy to  $dF(CF_3)ppy$ .

The dtbbpy ligand-centered redox process of the iridium(III) complexes is also shifted slightly, to a more positive value, when fluoro substituents are added to the cyclometalating ligand. Fluorine groups make the complex more electrophilic and, thus, easier to reduce. Since substituents on the cyclometalating ligand do not strongly affect the LUMO, the first ligand-centered redox process (dtbbpy) remains relatively unchanged.

Interestingly, a second ligand-centered redox wave is present in the CV of complex **1**, which does not appear for any of the other iridium(III) complexes (Figure 4). This peak corresponds to the  $dF(CF_3)ppy^{-/-2}$  process, addition of an electron to a vacant  $\pi^*$  orbital on the cyclometalating ligand (the coordinated cyclometalating ligand is intrinsically anionic). In the present study, the potential window is limited to  $\pm 2$  V by the solvent, but presumably, this second reduction wave as well as a third one would be discernible for all of these complexes if broader scanning conditions were attainable.

The low lying  $\pi^*_{CAN}$  orbital in the CV of complex **1** suggests a more prominent role for the <sup>3</sup>LC ( $\pi_{CAN} \rightarrow \pi^*_{CAN}$ )

Table 2. Redox Properties of Iridium Complexes<sup>a</sup>

complex	$E^0$ Ir <sup>III</sup> /Ir <sup>IV</sup> (V vs SCE)	$\Delta E_p$ (mV)	$E^0$ L/L <sup>-</sup> (V vs SCE)	$\Delta E_p$ (mV)	$\Delta E(\text{Ir}^{\text{III/IV}}-\text{L}^{0/-})$ (V)
[Ir(ppy) <sub>2</sub> (dtbbpy)] <sup>+</sup>	+1.21	65	-1.51	65	2.72
[Ir(Fmppy) <sub>2</sub> (dtbbpy)] <sup>+</sup>	+1.33	85	-1.50	70	2.83
[Ir(dFmppy) <sub>2</sub> (dtbbpy)] <sup>+</sup>	+1.49	75	-1.44	70	2.94
[Ir(dF(CF <sub>3</sub> )ppy) <sub>2</sub> (dtbbpy)] <sup>+</sup>	+1.69	105	-1.37/-1.68 <sup>b</sup>	70/110 <sup>b</sup>	3.06

<sup>a</sup> Cyclic voltammetry was carried out at 100 mV/s in 0.1 M TBAH/CH<sub>3</sub>CN at a Pt working electrode with a Pt counter electrode and Ag wire quasi-reference. Ferrocene was used as an internal standard and potentials are reported with respect to a saturated calomel (SCE) electrode. <sup>b</sup> For [Ir(dF(CF<sub>3</sub>)ppy)<sub>2</sub>(dtbbpy)]<sup>+</sup> both reduction of the dtbbpy ligand (at -1.37 V) and reduction of one of the dF(CF<sub>3</sub>)ppy ligands (at -1.68 V) were observed.

Table 3. Excited State Redox Properties of Iridium Complexes

complex	emission max (eV)	$E^0$ *IrL <sub>3</sub> <sup>3+/</sup> IrL <sub>3</sub> <sup>4+</sup> (V vs SCE)	$E^0$ *IrL <sub>3</sub> <sup>3+/</sup> IrL <sub>3</sub> <sup>2+</sup> (V vs SCE)
[Ir(ppy) <sub>2</sub> (dtbbpy)] <sup>+</sup>	2.17	-0.96	+0.66
[Ir(Fmppy) <sub>2</sub> (dtbbpy)] <sup>+</sup>	2.27	-0.94	+0.77
[Ir(dFmppy) <sub>2</sub> (dtbbpy)] <sup>+</sup>	2.41	-0.92	+0.97
[Ir(dF(CF <sub>3</sub> )ppy) <sub>2</sub> (dtbbpy)] <sup>+</sup>	2.58	-1.21	+0.89

transition in its mixed excited state and may contribute to the unique photoluminescent properties of this material. The redox trends that were observed within the [Ir(C<sup>^</sup>N)<sub>2</sub>(dtbbpy)]<sup>+</sup> series further suggest that the most heavily fluorinated complex (**1**) has the largest HOMO–LUMO gap and will exhibit the most blue-shifted emission. Additionally, the significant reducing strength of the excited state of complex **1**—see Table 3—suggests that it has the potential to be an extremely effective photocatalyst for hydrogen production.

**Static DFT Calculations.** Our electrochemical data was substantiated by the results obtained from static DFT calculations on the monocations of complex **1** and [Ir(ppy)<sub>2</sub>(dtbbpy)]<sup>+</sup>. The change in oxidation potential that was electrochemically observed for these two complexes is mirrored by changes in the calculated orbital energy of the HOMO. As shown in Figure 6, the HOMO, as well as HOMO-1 and HOMO-2 are strongly dominated by contributions from the metal d<sub>xy</sub>, d<sub>xz</sub>, and d<sub>yz</sub> orbitals, which is in accordance with ligand field theory. The associated e<sub>g</sub><sup>\*</sup>-like orbitals (calculations performed with a C<sub>2</sub> symmetry constraint) were over 6 eV higher in energy.

This large LFSE enabled tuning of the emission color to the blue region for iridium(III) complexes because the dominant emissive transition originates from a ligand-centered π\*-orbital (lower in energy than the metal-centered e<sub>g</sub><sup>\*</sup>-like orbitals). Because the vacant π\*-orbitals are localized on the ligands, their energy can be adjusted through deliberate chemical synthesis to allow for emission colors across the visible spectrum. Such a large d-orbital splitting is unattainable for second row transition metal ions, which makes ligand-based color-tuning in these complexes (e.g., Ru(bpy)<sub>3</sub><sup>2+</sup>) extremely difficult.

In both complex **1** and [Ir(ppy)<sub>2</sub>(dtbbpy)](PF<sub>6</sub>), the LUMO is almost exclusively located on the π-system of the dtbbpy ligand, as can be seen in Figure 6. No significant interaction between the ligand and the metal-centered orbitals can be observed in the LUMO, which explains the small effect of ppy substituents on the potential of the dtbbpy-based redox wave (B in Figure 4 and Table 2).

The DFT calculations also support the assumption that the second reduction wave is localized on the fluorinated

cyclometalating ligand. The LUMO+1 orbital is completely localized on the π-system of dF(CF<sub>3</sub>)ppy in complex **1** and is 0.24 eV higher in energy than the LUMO. The observed difference between the first and second reduction waves is comparable to this gap (0.31 eV). In contrast, the LUMO+1 obtained for the unfluorinated parent complex is much higher in energy than its LUMO (0.72 eV) and is located uniquely on the π-system of the dtbbpy ligand, which explains the absence of the second reduction wave in the CV of this compound. Last, an increase in the calculated HOMO–LUMO gap of the fluorinated complex is closely corroborated by the increase in emission energy (see Figure 2) and the difference in potential between the metal-centered and the dtbbpy-centered redox waves obtained through cyclic voltammetry (see Table 2).

#### Single-Layer Electroluminescent Device Performance.

The electroluminescence (EL) spectra of an ITO/complex **1**/Au device under forward bias (ITO positive with respect to Au) and under reverse bias are shown in Figure 2. The forward bias spectrum was the same in devices with a CsF/AI top contact. Interestingly, there is a slight blue shift in the EL peak, from λ<sub>max</sub> = 520 nm (CIE coordinates: x = 0.2607, y = 0.5555) to 500 nm (x = 0.1982, y = 0.5122), in going from positive to negative voltages. Such a shift in emission energy with bias direction has been observed previously in iridium(III) electroluminescent devices, the origin of which is not understood.<sup>15,16,23,26</sup> Similarly, the EL spectra are bathochromically shifted from the solution-based photoluminescence spectrum (Figure 2). As was the case for the thin film sample (photoluminescence), this shift can be attributed to self-quenching and increased overlap in the solid-state. The 500 nm emission of the device under reverse bias agrees with the photoluminescence maxima observed from the thin film and represents the lowest EL λ<sub>max</sub> reported for an iTMC-based device, to date.

The luminance and efficiency of devices based on complex **1** were found to depend on the direction of the bias, as well as on the choice of top contact. In general, devices with Au contacts showed poor device characteristics, namely, low luminance and high turn-on voltages, with luminance less than 10 cd/m<sup>2</sup> for voltages below 6 V. Light emission reached appreciable luminescence levels above 6 V. For example, at -6 V (ITO biased negatively) the current density, luminance, and quantum efficiency were 11 mA/cm<sup>2</sup>, 33 cd/m<sup>2</sup>, and 0.16%, respectively. The luminance half-life, the time to decay from maximum luminance to half-maximum, was 30 min for this device. With a CsF/AI top contact, only +3.5 V was required for significant luminescence. The current density, luminance, and quantum efficiency at +3.5 V were 1.7 mA/cm<sup>2</sup>, 40 cd/m<sup>2</sup>, and 0.75%, respectively, while the

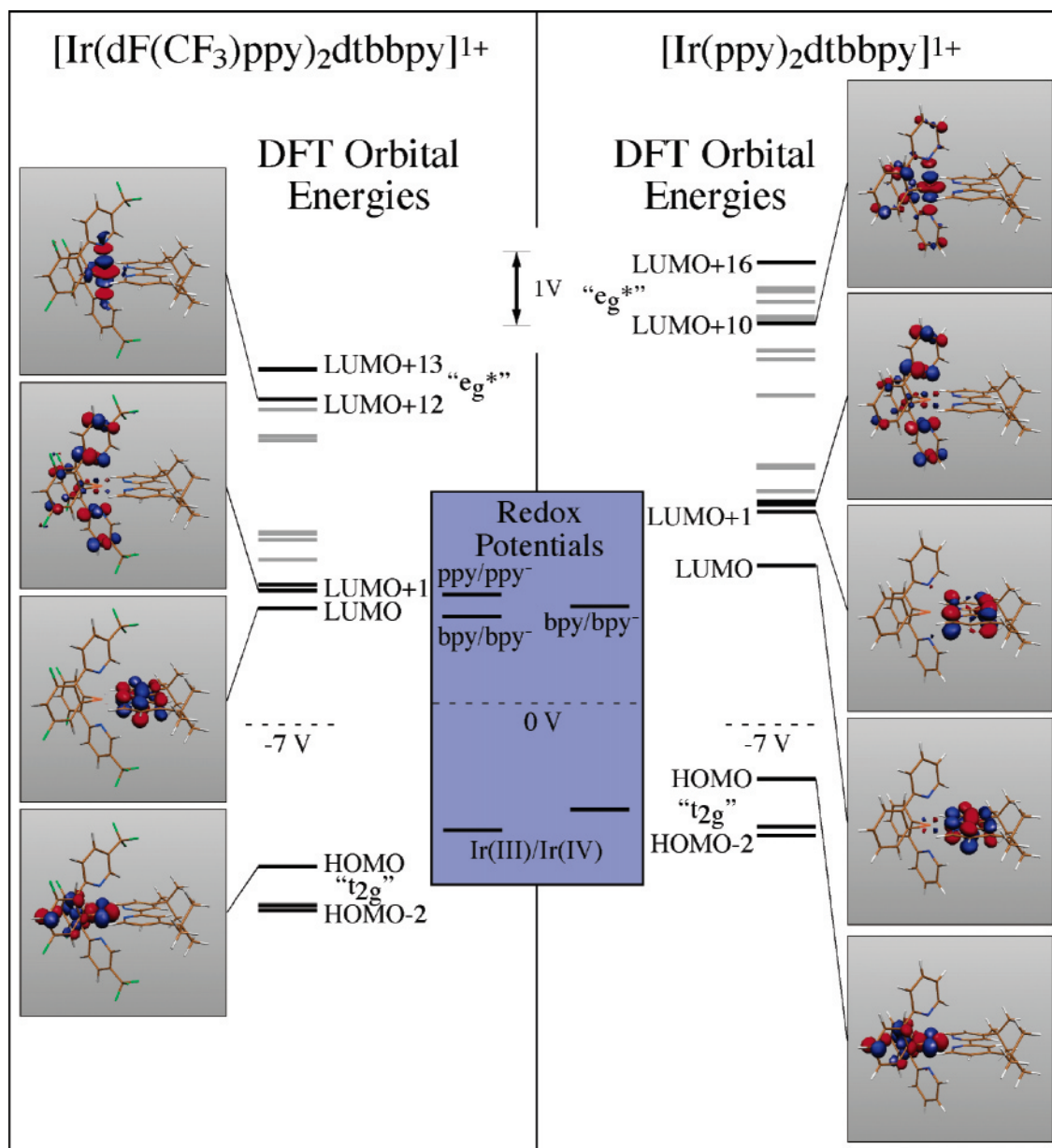


**Figure 6.** Molecular orbital diagrams obtained from DFT calculations: (left)  $[\text{Ir}(\text{dF}(\text{CF}_3)\text{ppy})_2(\text{dtbbpy})]^+$ , (right)  $[\text{Ir}(\text{ppy})_2(\text{dtbbpy})]^+$ , and (centered inset) Redox potentials obtained through cyclic voltammetry. The computed HOMO–LUMO gap is supported by experimental evidence.

luminescence half-life was 3.6 h. These devices do not show any emission under reverse bias due to electrochemical degradation of the CsF/Al contact. The improvement in device efficiency and turn-on voltage likely arises from the fact that CsF/Al has a significantly lower work function than ITO and Au, and hence is a better electron-injecting contact.

The low quantum efficiencies of these devices merit discussion. The EL external quantum efficiency ( $\eta$ ) of an OLED is given by<sup>55</sup>

$$\eta = b\varphi/2n^2 \quad (2)$$

where  $b$  is the recombination efficiency,  $\varphi$  is the fraction of excitons that decay radiatively, and  $n$  is the refractive index of the glass substrate (the factor  $1/2n^2$  accounts for the

coupling of light out of the device).<sup>55</sup> The  $b$  factor depends on the injection characteristics and is equal to unity when both contacts are ohmic. Since emission in these materials arises from the triplet state and singlet excitons are efficiently converted to triplets, the solid-state PL efficiency  $\varphi$  should be equal to the solid-state photoluminescence quantum yield. For the glass substrate,  $n = 1.5$ , making the factor  $2n^2$  equal 4.5. Neither  $b$  nor  $\varphi$  is directly known, but the product  $b\varphi$  is known and is equal to  $(2n^2)\eta$ , or approximately  $(4.5)\eta$ . As the maximum  $\eta$  was found to be 0.75% (for CsF/Al contacts), the maximum product  $b\varphi$  was found to be 0.034. The photoluminescence quantum yield, as found in solution, was 68% or 0.68, suggesting an upper bound of  $b\varphi = 0.68$ . This suggests that either  $b$  is considerably less than unity even for ITO/complex 1/CsF/Al devices or significant quenching of the photoluminescence occurs in going from solution to the solid-state film, or both. Advances in understanding of the injection and solid-state film properties of

(55) This is a first-order approximation that ignores charge trapping and field-dependent mobilities. Scott, J. C.; Malliaras, G. G. In *Conjugated Polymers*; Hadziioannou, G., van Hutten, P. F., Eds.; Wiley-VCH: New York, 1999; Chapter 13.

**Table 4. Photocatalytic Hydrogen Production**

photosensitizer	hydrogen produced ( $\mu\text{mol}$ )	relative quantum yield <sup>a</sup> ( $\mu\text{mol}$ )
$\text{Ru}(\text{dmphen})_3^{2+}$	145	145
$[\text{Ir}(\text{dF}(\text{CF}_3)\text{ppy})_2(\text{dtbbpy})]^+$	265	2025

<sup>a</sup> Relative quantum yield is equal to  $(\mu\text{mol hydrogen produced})/(1 - 10^{-\text{Abs}(465 \text{ nm})})$ .

devices based on complex **1** could lead to significant improvements in the external quantum efficiency.

**Photogeneration of Hydrogen.** Previous work in our group has demonstrated that heteroleptic, cyclometalated iridium(III) complexes can serve as extremely efficient photosensitizers for the photocatalyzed reduction of water to hydrogen.<sup>10</sup> The long excited-state lifetime of complex **1** ( $\tau = 2.3 \mu\text{s}$ ) and the highly reducing nature of this excited state (1.21 V, Table 3) suggest that complex **1** might also be an effective photosensitizer. Moreover, our previous results have indicated that iridium(III) complexes with fluorinated phenylpyridine ligands are better photosensitizers than their unfluorinated analogues.<sup>10</sup> The photocatalytic properties of complex **1** were investigated using the system described by Krishnan et al.,<sup>13</sup> consisting of complex **1**, an electron relay ( $\text{Co}(\text{bpy})_3\text{Cl}_2$ ) and a sacrificial reductant (triethanolamine) in a 1:1 solution of water:acetonitrile. For comparison purposes,  $\text{Ru}(\text{dmphen})_3(\text{PF}_6)_2$  was also used as a photosensitizer in this system. It has been shown that, in this system,  $\text{Ru}(\text{dmphen})_3^{2+}$  is a more effective photosensitizer than the commonly used  $\text{Ru}(\text{bpy})_3^{2+}$ .<sup>10,56</sup> The results from these experiments can be seen in Table 4, and it is clear that complex **1** is an excellent photosensitizer.

The molar extinction coefficient of complex **1** is  $180 \text{ M}^{-1} \text{ cm}^{-1}$ , as compared with that of  $\text{Ru}(\text{dmphen})_3^{2+}$ , which is over  $12\,000 \text{ M}^{-1} \text{ cm}^{-1}$ .<sup>20,53</sup> The amount of light absorbed by complex **1** is approximately  $1/8$  of that absorbed by

$\text{Ru}(\text{dmphen})_3^{2+}$ , yet complex **1** produces considerably more hydrogen. This is reflected in the relative quantum yields shown in Table 4. Our previous work demonstrated an iridium(III)-based photosensitizer with approximately 7 times the relative quantum yield of hydrogen compared to the  $\text{Ru}(\text{dmphen})_3^{2+}$  standard,<sup>10,56</sup> but the performance of complex **1** is dramatically better, with a relative quantum yield of hydrogen 14 times larger than that of the standard. We ascribe this result to a combination of the long lifetime and the significant reducing power of the excited state of complex **1**. Detailed photophysical, photochemical, and electrochemical studies are currently underway to gain a more complete understanding of factors governing the impressive behavior of this novel photosensitizer.

## Conclusion

We have reported the synthesis of a novel iTMC (complex **1**) containing 2 equiv of a multifluorinated cyclometalating ppy ligand and 1 equiv of a charge-transport enhancing dtbbpy ligand. The resulting iridium(III) complex is endowed with interesting redox and photophysical properties that enable its application as a chromophore in single-layer electroluminescent devices and as a photosensitizer in photocatalytic processes (e.g., hydrogen production). The blue-green electroluminescent emission (500 nm) and relative quantum yield of hydrogen ( $2025 \mu\text{mol H}_2$ ) reported herein mark the highest values to date.

**Acknowledgment.** This work was supported by the National Science Foundation (Career Award No. CHE-0449755), the Princeton Center for Complex Materials, and the Cornell Center for Materials Research, which are Materials Research Science and Engineering Centers of the National Science Foundation (DMR-9632275 and DMR-0213706), and a Camille and Henry Dreyfus Foundation New Faculty Award. We would also like to thank Andrew B. Bocarsly for the use of a potentiostat. J.D.S acknowledges support by a National Science Foundation Graduate Research Fellowship.

CM051312+

(56) Amouyal, E. In *Homogeneous Photocatalysis*; Chanon, M., Ed.; John Wiley & Sons: Chichester, U.K., 1997; p 263.